On the occurrence of stable and supersaturated metastable states in metallic core-shell nanoparticles

O. A. Oviedo, M. M. Mariscal and E. P. M. Leiva*

Received 19th November 2009, Accepted 10th February 2010
First published as an Advance Article on the web
DOI: 10.1039/b924348h

Following the framework established by Hill and Chamberlin [T. L. Hill and R. V. Chamberlin, *Proc. Natl. Acad. Sci. U. S. A.*, 1998, **95**, 12779] to analyze the extension of thermodynamics of small systems to metastable states, we have adopted the same basic ideas to study the thermodynamic stability of core-shell nanoparticles. For the first time we are able to address the question of whether or not core-shell nanoparticles have a limit of stability when they are under oversaturation conditions. By the latter, we mean the excess of chemical potential of the adsorbate (shell) atoms with respect to its bulk material, which is the driving force for nanoparticle growth. In this situation the probability density exhibits multiple local maxima associated with different core-shell metastable states. The decrease of the free energy barriers for the growth of the bulk phase of the shell material is analyzed for increasing oversaturation. At large positive oversaturations, the barrier disappears and the core-shell NP become unstable with respect to the bulk deposit of the shell material. A brief discussion on the model is made illustrating its application to a specific system by means of computer simulations using realistic interatomic potentials. One of the most striking results of these specific studies is the occurrence or not of a core-shell under undersaturation conditions depending on nanoparticle size.

Introduction

The special properties of nanocrystals have awakened great interest in both scientific and technological communities, and the size dependence of their thermodynamic properties has been a topic of intensive research in recent years.[1,2] These properties make it possible for the design of new devices and circuits of nanometric size. For example, nanoparticles (NP) are promising for optical, electronic, catalytic, and biomedical applications such as single electron tunneling devices, nanolithography, CO/CO_2 catalysts, and antibody sensors among others. Some applications related to biology, catalysis, and nanotechnology can be found in the revision articles by Ferrando *et al.*[3] and M. C. Daniel *et al.*[4]

NP exhibit very interesting size-dependent properties that cannot be achieved using their bulk counterparts. For novel applications, the synthesis of particles with a highly uniform distribution in size and shape, that is, ''monodispersed nanoparticles'', is of key importance. In this sense, much progress has been made over the last decade for both wet and dry methods of the synthesis of NP.[5] Mechanistic studies have shown that crystal size is mainly determined by the nucleation and growth process combined with the subsequent diffusion-controlled growth phenomenon.[6] However, while extensive fundamental and practical experience has been collected on the fabrication of nanoparticles, it is still not easy to obtain monodisperse systems required for some specific processes, since multiple factors have decisive influence in the monodispersity and other relevant characteristics of the nano system.[7]

Terrell Hill has undoubtedly been one of the pioneers in studying the thermodynamic properties of small systems,[8] long before the ''*nano*'' word was coined in the scientific literature. This author was the one who in the early 60s, moved by the behavior of proteins, amino acids, *etc.*, analyzed the behavior of small systems, making a parallelism with macroscopic thermodynamics. This branch of thermodynamics, then called nanothermodynamics (NT), is currently applied to systems of low dimensionality and/or systems of nanometric size. Perhaps the most remarkable result of NT is that the free energy is no longer a homogenous first order function of the extensive parameters, a fact that determines the loss of some useful thermodynamic equivalences. For example, in NT the traditional Gibbs–Duhem relationship disappears. A small system presents one more degree of freedom than their macroscopic counterparts, so that some properties formerly intensive depend in NT on the number of particles.

The surface energy, related to the energetic difference between the surface atoms and the interior ones, is one of the basic quantities to understanding surface structures, reconstructions, roughening, relaxations and size dependence of the thermodynamic parameters.[7,8] In this framework, the contribution of Hill and Chamberlin[9] to the description of metastable states (MS), is particular relevant for the present work. Fortunately, it comes out that the rules describing stable equilibrium states (SS) remain the same for nanometric systems,[8] so that they can be obtained by entropy maximization or minimization of the suitable thermodynamic potential for each ensemble. A MS is one that presents a critical point in the

INFIQC, Departamento de Matemática y Física, Facultad de Ciencias Químicas, UNC. Argentina. E-mail: eleiva@fcq.unc.edu.ar, marmariscal@fcq.unc.edu.ar, ooviedo@fcq.unc.edu.ar; Tel: +54 (0351)4344971

entropy (free energy), but without corresponding to a global maximum (minimum). Using a simple model, Hill and Chamberlin[9] showed that boundary effects (surfaces, contours, *etc.*) may be responsible for the existence of MS. In that work, it was shown that a proper analysis of these MS must be done taking into account mathematical divergences and physical convergences of the partition function. An accurate description of the thermodynamic properties of nanoparticles should include a correct description of their surface energy.

Concerning metallic NP, Jiang *et al.*[10] have analyzed theoretical nucleation of a metal on a surface of the same material, examining the free energy landscape using a drop model. In that treatment for nucleation, the nucleus was assumed to be spherical and the free energy of a cluster was analyzed as a function of radius and temperature. Jiang *et al.* introduced the size-dependence using a Laplace–Young equation ($\Delta P = 2\gamma/r$) finding good agreement with experimental results. A similar approach was performed by Wang *et al.*[11] to elucidate diamond nucleation. However, when a liquid is cooled below its freezing temperature, the nucleation requires the formation of a new stable phase (solid) that introduces an energetically unfavorable solid–liquid interface and therefore creates a free energy barrier between phases. Mendez-Villuendas *et al.*[12] addressed this issue under the formalism of statistical mechanics using the critical size of the largest solid-type embryo as an order parameter. In such work, they analyzed the free energy profiles as a function of the order parameter at different temperatures. At temperatures relatively close to the melting point, the free energy function has a minimum for small size values that indicates the presence of a metastable state. When the temperature decreases, the free energy becomes monotonically decreasing, indicating that the metastable state has exceeded its limit of stability.

In the case of electrochemical synthesis of nanoparticles the key parameter to control the behavior of the system is usually not the temperature but the redox potential, since it allows the control of the chemical potential of the metal constituting the nanoparticle. In this respect, Plieth[13] found a shift of the reversible redox potential with nanoparticle size that was explained using an expression analogous to the Kelvin equation, thus predicting that these changes are inversely proportional to the radius of the NP.

The most remarkable differences between liquid and solid surfaces are the surface energy (γ) and the surface stress (σ). γ describes the reversible work per unit area to form a new surface while σ denotes the reversible work per unit area due to elastic deformation, which is equal to the derivate of γ with respect to the tangential strain to the surface.[14] Rusanov and Shchekin[15] have tackled this problem and they have improved the model including explicitly different γ and σ, this contribution extended Gibb's formula to monometallic nanoparticles. In this model the chemical potential is a function of curvature, γ and σ.

In the case where the chemical nature of the metal to be deposited is different from that of the surface, electrode potential (or that of a redox couple) may be used to control the coverage degree of foreign adatoms.[16] In a previous work,[17] we presented a thermodynamic analysis and computer simulations corresponding to the electrochemical formation of pure and core-shell bimetallic nanoparticles. The behavior of those systems where the binding energy of the adsorbate to the substrate is more positive than that of the bulk adsorbate showed close similarities to the behavior expected for the growth of pure metal nanoparticles.[17,18] However, when the adsorbate–substrate interaction is stronger than the bulk interaction of the adsorbate material, a manifold of behavior arises depending on NP size and shape.[17]

In the present contribution, we follow the framework established by Hill and Chamberlin,[9] and develop a statistical mechanical approach to extend our previous thermodynamics analysis of core-shell NP to study the role of MS in these systems. A brief discussion on the model is made illustrating its application with computer simulations using realistic semi-empirical interatomic potentials.

The model and calculation method

In the following we adhere to the notation used by Hill *et al.*[9,19] in order to assemble a statistical mechanical description of the problem that we tackled in our previous work concerning the formation of metallic core-shell NP under chemical potential control.[17]

Fig. 1 shows a scheme of the model system. For the present purpose, we consider an ensemble of small incompressible bimetallic NP immersed in a liquid solution containing ions of the species being deposited onto a seed NP. Without loss of generality, since the same approach could be used to study the formation of alloyed NP, we assume that these clusters are made of two components, Me and S, arranged in such a way that the system is made of small core(S)/shell(Me) aggregates.

We also assume that the concentration of these small metallic aggregates is small enough to neglect the interactions among them.[19]

The grand canonical partition function of a single conglomerate $\Upsilon(\mu_{Me}, N_S, T)$ is related to the corresponding canonical partition function $Q(n_i, N_S, T)$ through:[8,9]

$$\Upsilon(\mu_{Me}, N_S, T) = \sum_{n_i=1}^{\infty} Q(n_i, N_S, T) \exp\left[\frac{n_i \mu_{Me}}{kT}\right] \qquad (1)$$

where k is Boltzmann's constant and n_i is the number of Me atoms deposited on S. In principle, the sum runs over all positive integers but we will find that with practical purposes it can be drastically reduced on physical grounds, as proposed by Hill and Chamberlin.[9]

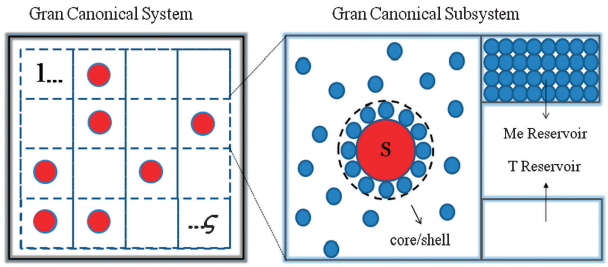

Fig. 1 Schematic representation of the ensemble employed to study core-shell NP growth. In the present model, the coverage is a function of the size of the NP core (N_S), the temperature (T), and the chemical potential of the Me species (μ_{Me}).

In order to write eqn (1) in a more suitable form, we will consider that the Helmholtz free energy of the bulk metal Me, say F^0_{Me}, can be written in terms of its partition function Q^0 (N_{Me}, T) according to:

$$F^0_{Me} = -kT \ln Q^0(N_{Me}, T) \quad (2)$$

In the case of a piece of bulk metal Me made of N_{Me} atoms, the chemical potential of Me in this limit, say μ^0_{Me}, is given by:

$$\mu^0_{Me} = \frac{F^0_{Me}}{N_{Me}} \quad (3)$$

Thus, the free energy of a piece of bulk made of n_i metal Me atoms, will be given by:

$$F^0_{Me,n_i} = n_i \mu^0_{Me} \quad (4)$$

With this in sight, we can rewrite eqn (1) as:

$$\Upsilon(\mu_{Me}, N_S, T) = \frac{Q^0(N_{Me}, T)}{Q^0(N_{Me}, T)} \Upsilon(\mu_{Me}, N_S, T) = \sum_{n_i=1}^{\infty} \exp\left[-\frac{F_{n_i}}{kT} + \frac{n_i \mu_{Me}}{kT} + \frac{F^0_{Me,n_i}}{kT} - \frac{n_i \mu^0_{Me}}{kT}\right] \quad (5)$$

That can be rearranged to yield:

$$\Upsilon(\mu_{Me}, N_S, T) = \sum_{n_i=1}^{\infty} \exp\left[-\frac{F_{n_i} - F^0_{Me,n_i}}{kT} + \frac{n_i \Delta\mu_{Me}}{kT}\right] \quad (6)$$

where we have defined the quantities: $\Delta\mu_{Me} = \mu_{Me} - \mu^0_{Me}$ and $F_{n_i} = -kT \ln Q(n_i,N_S,T)$. Thus, $\Delta\mu_{Me}$ represents an excess of chemical potential with respect to the chemical potential of the bulk Me material.

On the other hand, we can multiply and divide by the canonical partition function of the core Q_S (N_S,T) = exp ($-F_S/kT$) (made only of the metal S):

$$\Upsilon(\mu_{Me}, N_S, T) = \exp\left[-\frac{F_S}{kT}\right] \sum_{n_i=1}^{\infty} \exp\left[-\frac{F_{n_i} - F^0_{Me,n_i}}{kT} + \frac{n_i \Delta\mu_{Me}}{kT} + \frac{F_S}{kT}\right] \quad (7a)$$

$$\Upsilon(\mu_{Me}, N_S, T) = A \sum_{n_i=1}^{\infty} \exp\left[-\frac{\Delta F_{n_i}}{kT} + \frac{n_i \Delta\mu_{Me}}{kT}\right] \quad (7b)$$

where F_S is the Helmholtz free energy of the core and we have defined $\Delta F_{n_i} = F_{n_i} - F_S - F^0_{Me,n_i}$ and $A = \exp(-\beta F_S)$. Note that ΔF_{n_i} corresponds to the excess of free energy of the Me type atoms in the cluster referred to the bulk metal Me.

In the case of electrochemistry, the excess of chemical potential, $\Delta\mu_{Me}$ associated with oversaturation (if positive) or undersaturation (if negative) is related to an overpotential η measured with respect to a reference electrode of the same metal Me in the same solution.[20] Thus, for electrochemical applications we should replace $\Delta\mu$ by $-zF\eta$, where z is the valence and F is the Faraday constant. In electrochemical jargon, $\eta > 0$ corresponded to underpotential deposition (UPD) conditions, while $\eta < 0$ (OPD) corresponded to overpotential deposition. However, the same concepts would be applied to the case of crystal growth of a surface in contact with its vapour; in such a case the excess of chemical potential is related to an increment of the pressure in the vapour phase.[19]

Eqn (7b) allows in principle the calculation of all the properties of the system but its straightforward use is prohibitive because of the huge number of terms (in principle infinite) involved in the sum. In order to tackle a particular type of system, we will make some assumptions, which follow in some aspects the treatment given by Hill and Chamberlin[9] to deal with liquid-like clusters. Furthermore, we will apply it to a similar model system to the one we have analyzed previously on thermodynamic grounds,[17] namely that of a core-shell NP. The ΔF_{n_i} values in the sum (eqn (7b)) involve the canonical partition function of the core-shell system for a different number of adsorbate atoms, which also includes a very large number of configurations. In order to circumvent this calculation for liquid clusters, Hill and Chamberlin[9] introduced a surface energy term, which was proportional to the number of surface atoms of the clusters, so that a single term was considered for the canonical partition function. In the present work, we attempt the calculations of ΔF_{n_i} considering different contributions to it, namely, static (configurational), vibrational, rotational, and translational.

To proceed further, we write:

$$\Delta F_{n_i} = \Delta U_{n_i} - T\Delta S_{n_i} \approx [\Delta U^s_{n_i} + \Delta U^v_{n_i} + \Delta U^r_{n_i} + \Delta U^t_{n_i}] - T[\Delta S^s_{n_i} + \Delta S^v_{n_i} + \Delta S^r_{n_i} + \Delta S^t_{n_i}] \quad (8)$$

where the upper indices s, v, r, and t denote static, vibrational, rotational, and translational contributions and we have defined:

$$\Delta U^j_{n_i} = [U^j_{n_i} - U^{0,j}_{Me,n_i} - U^j_S] \quad (9)$$

and,

$$\Delta S^j_{n_i} = [S^j_{n_i} - S^{0,j}_{Me,n_i} - S^j_S] \quad (10)$$

the subscripts: n_i,(Me,n_i) and S denote the core-shell, pure metal Me and substrate contributions, respectively. The symbol $\approx$ in eqn (8) denotes that the coupling between the different contributions has been neglected and they are considered additive.

With the purpose of making calculations for a model system at room temperature, we make the following assumptions: the static energy terms on eqn (8) were obtained from embedded atom calculations,[21] choosing a minimum energy configuration for a given n_i. Thus, $U^S_{n_i}$ and U^S_S involve minimum energy calculations for a core(S)–shell(Me) and a pure core(S), respectively, while $U^{0,S}_{Me,n_i}$ corresponds to the energy of n_i bulk atoms of Me. The vibrational contribution $\Delta U^v_{n_i}$ was neglected. This is tantamount to assume that the vibrational status of the Me atoms in the shell is similar to that of the Me atoms in the bulk. The corresponding assumption for the core atoms is that they behave vibrationally the same way, independent of whether they are covered by the shell atoms or not. Although this is strictly not true, this contribution should be negligible at room temperature as compared with $\Delta U^s_{n_i}$. In fact, comparison between static[22] and quasi-harmonic lattice

calculations[23] for metal monolayers deposited on foreign surfaces indicate that the vibrational contribution to the energy excess is a fraction of kT for small lattice misfits and relatively compact surfaces ((111) and (100)). A similar consideration can be made for the excess contribution $\Delta S^{v}_{n_i}$. In this respect, Chui *et al.*[24] have considered different structures of Au–NP (perfect icosahedra, icosahedra with defects and amorphous NP between 2 nm and 8 nm) calculating entropic vibrational contributions using EAM potentials in the harmonic approximation. These authors found that the vibrational entropy contributes 2% to the free energy of the system, independent from the shape and size of the NP. However, there are in the literature other results showing that solid–solid transformations in nanoparticles can be caused by vibrational entropy contributions.[25] This opens up many possibilities involving calculations similar to those undertaken here but with different cluster morphologies. However, the transition between different morphologies can only occur surmounting an important energy barrier.[26] For example, experiments with Au nanoparticles show that these must be heated to temperatures close to the melting point for these transitions to occur.[27] Since we consider here ordinary electrochemical conditions, where experiments are driven at room temperature, we expect that these transitions should not play an important role. Increasing temperatures could lead to structural transformations that would make the calculations more complicated, but the main physical features of the model will be retained.

Concerning $\Delta U^{r}_{n_i}$, we performed approximate calculations by assuming a spherical cluster. Using eqn (9), we get for $\Delta U^{r}_{n_i}$:

$$\Delta U^{r}_{n_i} = U^{r}_{n_i} - U^{r}_{S} \tag{11}$$

In the classic approximation, this quantity is equal to zero.[8]

The entropic counterpart is in turn:[8]

$$\Delta S^{r}_{n_i} = S^{r}_{n_i} - S^{r}_{S} \tag{12}$$

with:

$$S^{r}_{n_i} = k \ln\left(\frac{4\pi^2 I_{n_i} kT}{h^2}\right) \tag{13a}$$

$$S^{r}_{S} = k \ln\left(\frac{4\pi^2 I_{S} kT}{h^2}\right) \tag{13b}$$

where the subscripts n_i and S denote core-shell and core, and I_{n_i} and I_S are the moment of inertia of the core-shell and core, respectively; h denotes Planck's constant.

Concerning the classical translational energy contribution, it can be easily shown that it is equal to zero[8] and the entropic term is:

$$\Delta S^{t}_{n_i} = S^{t}_{n_i} - S^{t}_{S} \tag{14}$$

with:

$$S^{t}_{ni} = k\ln[(2\pi(N_S m_S + n_i m_{\mathrm{Me}})kT)^{3/2}\, h^{-3}\, Ve^{5/2}] \tag{15a}$$

$$S^{t}_{S} = k\ln[(2\pi(\mathrm{N_S m_S kT})^{3/2}\, h^{-3}\, Ve^{5/2}] \tag{15b}$$

where m_{Me} and m_S are the masses of Me and S atoms, respectively, and V is the volume.

The static entropic contribution

$$\Delta S^{s}_{n_i} = S^{t}_{n_i} - S^{t}_{S}$$

will be also neglected. To test the accuracy of this approximation, we have performed the exploratory calculations described in the Appendix. There, we show that this contribution should be of the order of 0.3 eV at room temperature.

With the purpose of computing the static energy contributions to the free energy, we followed the following routine: different Au-core structures were built cutting a piece of Au *fcc* bulk structure, on which the Ag atoms were located. Truncated octahedron (TO) NP shapes were selected. We considered the first four members of the TO family, that is, TO_38, TO_201, TO_586, and TO_1289, where the number makes reference to the quantity of atoms constituting the NP core. For a given number of deposited atoms on the cluster serving as substrate, the minimum energy configuration was determined by choosing the lowest energy configuration for each adatom added to the system followed by a low temperature simulated annealing. The formation of alloys was not allowed in the present studies. In principle, this is an approximation. However, recent experiments show that meticulous control of a metallic shell of Ag on Au is possible at the single monolayer level,[28] with no indication of massive alloying in the high resolution TEM images, where core and shell boundaries appear well defined. In order to explore regions of the configuration space close to those visited in electrochemical experiments at room temperature, the simulated annealing procedure was started at 300 K and finished at 0 K. This was made so for two reasons: on one side, most electrochemical experiments are made at this temperature, so that during the annealing procedure the system initially has access to the same energy landscape as in the experiments. Increasing the initial temperature would lead to some artificial alloying formation that would not be found in the room-temperature experiments. On the other hand, we finish the annealing at 0 K since in the calculations described below we divide different contributions to the free energy into "static" and thermal parts. Thus, the static parts refer to the results at 0 K and thermal contributions will be approximated using semi-classical approximations. An analytical embedded atom model was used to compute the interaction between the particles.[21] This semi-empirical potential provides a reasonable description of the many-body interactions present in metallic systems. For further details on the simulation technique the reader may follow ref. 17.

Results and discussion

We analyze in the first place the rotational and translational contributions. As mentioned above, the rotational and translational energy excesses referred to the bulk state are zero, and the entropic parts can be simply calculated through the

moment of inertia according to:[8]

$$\Delta S^{r}_{n_i} = k \ln\left(\frac{I_{n_i}}{I_S}\right) \approx k \ln(1 + \mathrm{MR}^{r}) \qquad (16)$$

$$\Delta S^{t}_{n_i} \approx \frac{3}{2} k \ln(1 + \mathrm{MR}^{t}) \qquad (17)$$

where $M = m_{\mathrm{Me}}/m_S$ is the mass ratio. $R^r = (r^5_{n_i} - r^5_S)/r^5_S$ and $R^t = (r^3_{n_i} - r^3_S)/r^3_S$ are the form factors of the rotational and translational contributions, r_{n_i} and r_S are the radius of the core-shell and naked core, respectively.

Eqn (16) and (17) are obtained assuming a spherical shape of the particle and similar atomic volumes for Ag and Au ($r_{\mathrm{Au}} = 0.136 \pm 0.006$ nm and $r_{\mathrm{Ag}} = 0.145 \pm 0.005$ nm). Note that (16) and (17) depend on neither the volume nor on the temperature of the system, although eqn (13) and (15) do.

Table 1 shows the rotational and translational entropic contributions at 300 K for the case of Ag deposition on Au NPs of different sizes. The crystallographic average radius of TO structures containing 586, 1289 and 2406 was *ca.* 1.22 nm, 1.63 nm and 2.04 nm, respectively, while the thickness of the Ag deposit on these surfaces was assumed to be that of one, two and three monolayers, respectively. The rotational entropic contributions are more important than the corresponding translational entropic ones, and in all cases the values are of the order of a few meV at room temperature. The rotational and translational entropy excesses increase with the thickness of the shell and decrease with the size of the core.

Fig. 2a shows the static energy contributions, corresponding to Ag deposition on Au(TO_1289). In the first place, it is worth noting that the $\Delta U^s_{n_i}$ values are in the order of hundreds of eV, rapidly increasing with increasing thickness of the shell. This quantity represents the largest contribution to the free energy. A close inspection of this plot shows that the energy of the system presents a global minimum before the completion of the monolayer. This minimum occurs at $n_i = 480$, corresponding to a coverage of 75% of the monolayer, a behaviour that could not be described by a continuum theory of nucleation and growth. The physical reason for this behavior is very simple: the energetically stable structure for the decorated cluster at $\Delta\mu_{\mathrm{Me}} = 0$ is where the [111] and [100] facets have been covered, while the edges remain uncovered, since the adatoms have a lower coordination here.

However, we note that this situation could be quantitatively (but not qualitatively) altered for NP with different morphologies (*i.e.* decahedra, icosahedra, cubooctahedral, *etc*).

Table 1 Rotational (top) and translational (bottom) entropic excess contributions at 300 K for the case of Ag deposition on different Au-NP at different thicknesses, corresponding to one, two and three monolayers. All values are given in meV

$T\Delta S^t$	TO_586	TO_1289	TO_2406
One monolayer	0.12	0.11	0.10
Two monolayers	0.18	0.15	0.13
Three monolayers	0.24	0.20	0.17
$T\Delta S^r$	**TO_586**	**TO_1289**	**TO_2406**
One monolayer	0.04	0.03	0.02
Two monolayers	0.07	0.05	0.04
Three monolayers	0.11	0.08	0.06

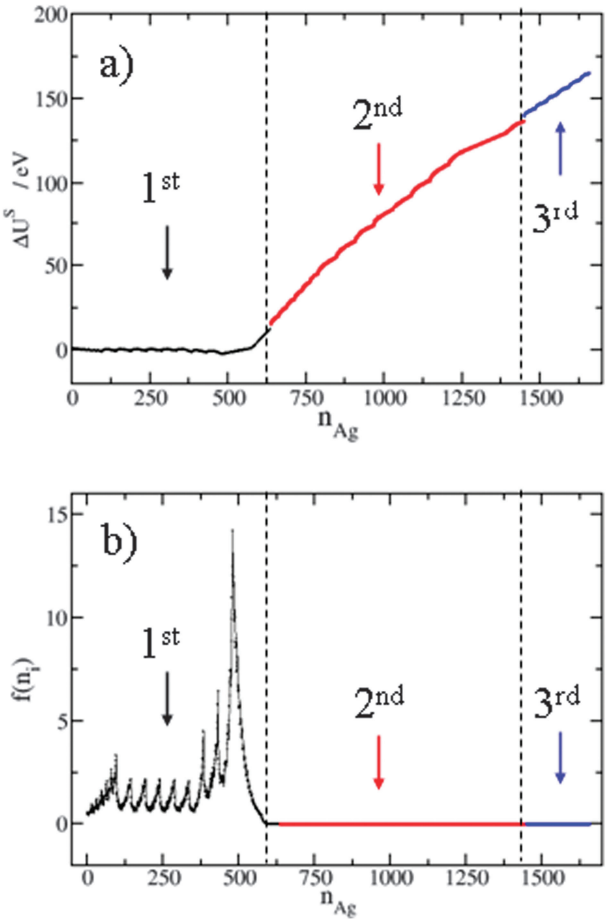

Fig. 2 (a) Static energy excess and (b) probability density to have n_{Ag} atoms deposited on Au(TO_1289) as a function the number of Ag atoms forming the shell at zero excess of chemical potential. The lines correspond to formation of: the first (black), the second (red) and the third (blue) adlayers.

The probability density to have n_i atoms of Me-type deposited on a cluster made of N_S atoms of S-type at the chemical potential μ_{Me} and temperature T is:

$$p_{n_i}(\mu_{Me}, N_S, T) = \frac{\exp\left[-\frac{\Delta F_{n_i}}{kT} + \frac{n_i \Delta\mu_{\mathrm{Me}}}{kT}\right]}{\Upsilon(\mu_{\mathrm{Me}}, N_S, T)} \qquad (18)$$

The previous equation shows that the location of maxima (minima) in the probability density does not depend explicitly on the partition function. In fact, the conditions for the existence of local maxima or minima in the probability density function are:

$$\Delta F_{n_{i,\max}-1} + \Delta\mu_{\mathrm{Me}} > \Delta F_{n_{i,\max}-1} < \Delta F_{n_{i,\max}-1} - \Delta\mu_{\mathrm{Me}} \qquad (19a)$$

$$\Delta F_{n_{i,\min}-1} + \Delta\mu_{\mathrm{Me}} > \Delta F_{n_{i,\min}-1} < \Delta F_{n_{i,\min}-1} - \Delta\mu_{\mathrm{Me}} \qquad (19b)$$

where $n_{i,\max}$ and $n_{i,\min}$ denote the number of shell atoms yielding maxima and minima probability densities, respectively. In the following and for visualization purposes, rather than plotting the functions $(p_{n_i}\Upsilon)$ or $\beta(-\Delta F_{n_i} + n_i\Delta\mu_{\mathrm{Me}})$, we will rather show the function defined by:

$$f(n_i) = (p_{n_i}(\mu_{\mathrm{Me}}, N_S, T)\,\Upsilon(\mu_{\mathrm{Me}}, N_S, T))^{\frac{1}{\beta}} \qquad (20)$$

which is monotonic with both of them and presents an extreme at the same points of their domain.

Fig. 2b shows $f(n_i)$ for Ag atoms deposited on a Au(TO_1289) cluster as a function on n_i for zero overpotential.

We see that $f(n_i)$ presents many minima and maxima, associated with the nucleation and growth process of two-dimensional phases on the facets of the NP(TO_1289). The largest maximum is associated with the completion of all facets [100] and [111]. Following this process we find a decrease of $f(n_i)$ due to the adsorption of Ag atoms at the edges of the facets, namely the [111]–[111] and [111]–[100] borders. At n_i = 636 the first monolayer of Ag on the Au–NP has been completed (end of the black curve); then a second layer is deposited on the first Ag monolayer (red curve in Fig. 2b). The subsequent adsorption processes have a lower probability of occurring (at overpotential zero), and even its limit is zero:

$$\lim_{n_i \to \infty} [p_{n_i}(\mu_{\mathrm{Me}}, N_S, T)]\Big|_{\Delta\mu_{\mathrm{Me}}=0^-, N_S, T} = 0 \qquad (21)$$

where $\Delta\mu_{\mathrm{Me}} = 0^-$ denotes that the limit is taken for a small undersaturation.

Thus, we conclude that the situation where n_i = 480 corresponds to a global minimum at zero excess of chemical potential. Under finite subsaturation conditions ($\Delta\mu_{\mathrm{Me}} < 0$) the limit of eqn (21) is also zero, but the maximum at n_i = 480 decreases (with respect to the other maxima). At a more negative $\Delta\mu_{\mathrm{Me}}$ there are other configurations ($n_i < 480$) that become eventually more stable and reach the status of global minimum. Fig. 3 shows the behaviour of $f(n_i)$ for different negative excesses of chemical potential. It is evident that in the range −4 meV < $\Delta\mu_{\mathrm{Me}}$ < 0 meV the global minimum corresponds to n_i = 480 (Fig. 3a). In the range −13 meV < $\Delta\mu_{\mathrm{Me}}$ < −4 meV the global minimum is found at n_i = 96 (Fig. 3b and c), corresponding to the decoration of [100] facets, while at $\Delta\mu_{\mathrm{Me}}$ < −13 meV the global minimum is at n_i = 0. Fig. 4 summarizes the general behaviour of $f(n_i)$ in the whole range of excesses of chemical potential considered here.

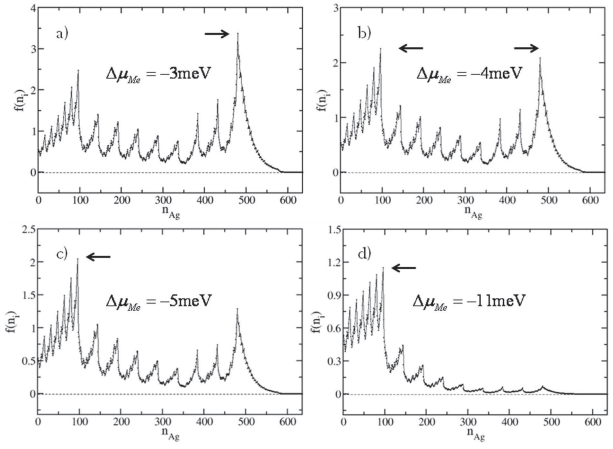

Fig. 3 Probability density of finding n_i Ag atoms deposited on Au(OT_1289) at different excesses of chemical potential. (a) −3 meV, (b) −4 meV, (c) −5 meV, and (d) −11 meV. The arrow shows the most relevant probability density peaks.

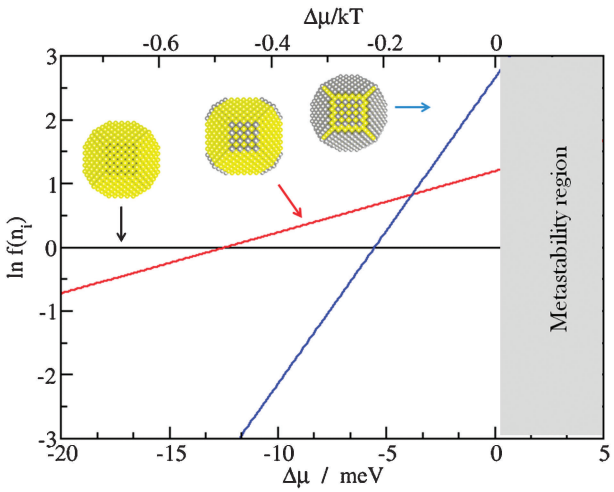

Fig. 4 Behavior of the function $f(n_i)$ monotonically related to the probability density of observing the three states n_i = 0, n_i = 98 and n_i = 480 as a function of the excess of chemical potential. The most stable structure at each chemical potential is given by the upper envelope of the lines. The upper scale corresponds to kT units. The metastability region of the core-shell structures is marked in grey.

For this Figure, we have selected three decoration states, corresponding to n_i = 0, n_i = 98 and n_i = 480. This choice was made because these three states are the predominant ones in the undesaturation range of the present system. The most stable structure at each chemical potential is given by the upper envelope of the lines. This behavior is expected according to that of adatom deposition on single crystal surfaces,[23] where it was found that this phenomenon occurs first on the more open surfaces.

We turn now to analyze the positive region of $\Delta\mu_{\mathrm{Me}}$, the OPD region. Fig. 5 shows the behaviour of $f(n_i)$ for different positive excesses of chemical potential, that is, for the region marked in grey in Fig. 4, corresponding to free energy calculations up to the third pseudomorphic Ag shell.

When the system is subject to a positive excess of chemical potential ($\Delta\mu_{\mathrm{Me}} > 0$), $f(n_i)$ grows rapidly. In the range 0 meV < $\Delta\mu_{\mathrm{Me}}$ < 35 meV the maximum is localized at n_i = 480

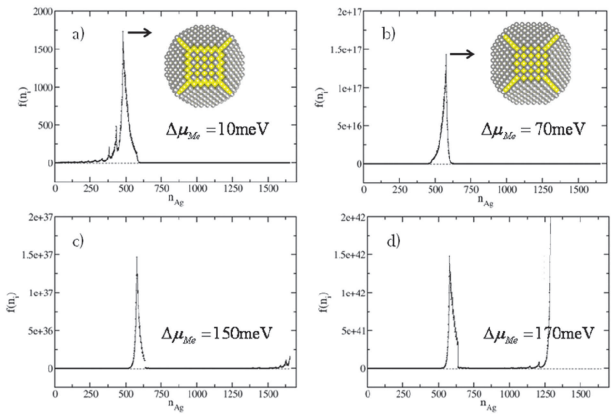

Fig. 5 Probability to have atoms n_i deposited on Au(OT_1289) at different excess of chemical potential. (a) 10 meV, (b) 70 meV, (c) 150 meV, and (d) 170 meV. The inset shows the structure of the core-shell at the point marked with the arrow.

(Fig. 5a), moving from $n_i = 480$ to $n_i = 576$ (Fig. 5b) when $\Delta\mu_{Me}$ changes only between 35 meV and 37 meV.

From the latter chemical potential, the maximum remains stable at $n_i = 576$. The latter state corresponds to a situation where the Ag atoms have covered all the [100] and all the [111] facets plus all the edges between [111] and [100] facets. The edges between neighbouring [111] facets remain unfilled. The frames corresponding to $n_i = 480$ and $n_i = 576$ are presented in the insets of Fig. 5a and b, respectively. The last point of the plots of Fig. 5 is $n_i = 1656$, which corresponds to the filling of all [100] facets with three pseudomorphic layers of Ag. It is well known from electrochemical experiments that the deposition of Ag on Au leads to one or two layers in the underpotential region,[16,18] but not to three. This shows that the third layer of Ag on Au is, with practical purposes, energetically indistinguishable from Ag bulk. This has also been confirmed by our calculations, where we find that the binding energy per atom for the formation of the third Ag layer on the second differs from the Ag bulk binding energy in less than 0.1%. Thus, we can take the onset of the formation of the third Ag layer as a measure for the beginning of the rise of $f(n_i)$ toward infinity and proceed with an analysis similar to that performed by Hill and Chamberlin[9] for the mathematical divergence of the probability density function.

In the range of positive excesses of chemical potential, eqn (21) is no longer valid but we have the limit:

$$\lim_{n_i \to \infty} [p_{n_i}(\mu_{Me}, N_S, T)]\Big|_{\Delta\mu_{Me}=0^+, N_S, T} = \infty \qquad (22)$$

In the framework of the study of a liquid cluster, Hill and Chamberlin[9] associated this limit with the massive growth of the liquid drop. Similarly, we can connect this limit with the growth of a bulk deposit of Me on the NP. This bulk deposit has the highest probability density, corresponding to the global free energy minimum. The term $\exp(\beta n_i \Delta\mu_{Me})$ in eqn (7b) is responsible for the divergence of the partition function in this situation. However, for relatively small but positive $\Delta\mu_{Me}$s ($\Delta\mu_{Me} \to 0^+$), the onset of the divergence of the probability density is located at relatively large n_i values (see Fig. 5c), separated from the most probable metastable state by a region where the probability density is (for practical purposes) negligible. As the overpotential increases, the divergence is shifted to lower values of n_i (see Fig. 5d), and consequently the region where the probability is negligible becomes thinner. This phenomenon is associated with a decreasing stability of the metastable core-shell structure. Hill and Chamberlin suggested that the low probability zone that separates the first peak from the divergence acts as a "bottleneck" separating the metastable structure from massive growth by a kinetic impediment.[9] In the following, we will characterize the magnitude of this bottleneck by two quantities: the ratio of the probability density of the largest local maxima p_{max} of Fig. 5 to the probability density of the lowest minimum p_{min} in the direction of the divergence, and the difference in the number of particles between these two extremes.

We will denote these quantities with $p_{rel} = p_{max}/p_{min}$ and $\Delta n = n_{min} - n_{max}$, where n_{max} and n_{min} are the number of

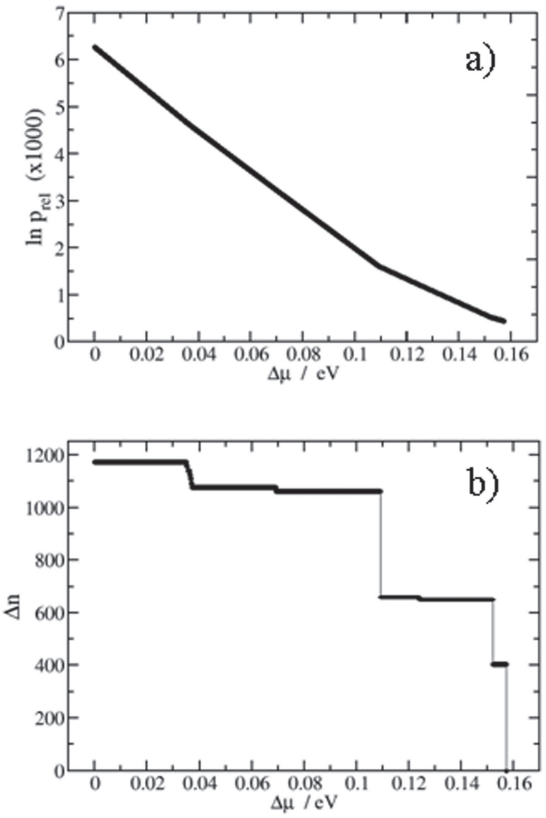

Fig. 6 (a) p_{rel} and (b) Δn as a function of the excess of chemical potential $\Delta\mu_{Me}$. p_{rel} and Δn are a measure for the width of a bottleneck separating the most stable metastable state from the bulk phase. Their meaning is described in the text.

adatoms in the cluster at p_{max} and p_{min}, respectively. Fig. 6 shows p_{rel} (a) and Δn (b) as a function of the excess of $\Delta\mu_{Me}$. It can be observed than an excess of chemical potential of 160 meV is translated into a change of the order of e^6 in p_{rel} and in a change of 10^3 in Δn. In other words, the bottleneck for the formation of the bulk phase can only be surmounted by the application of an overpotential of the order of 160 mV, which is a meaningful amount from the electrochemical viewpoint.

We turn now to consider the behavior of $f(n_i)$ for different core sizes (Fig. 7). There, it can be appreciated that the way in which the nanoparticle becomes decorated at $\Delta\mu_{Me} = 0$ is strongly dependent on particle size.

For example, when $N_S = 1289$ decoration of all the [100] and [111] facets is expected, since the maximum in the probability density is found at $n_{Ag} = 480$, which corresponds to this situation. On the other hand, for the remaining smaller Au cores (TO_{586}, TO_{201}, and TO_{38}) no decoration of the core occurs at all at $\Delta\mu_{Me} = 0$. In fact, for these smaller core sizes all maxima in $f(n_i)$ are smaller than 1. This corresponds to the non-occurrence of underpotential deposition in the electrochemical system. Thus, the present calculations show that the existence of underpotential deposition in nanoparticles may be size dependent. This can be interpreted as a curvature effect. The existence of a positive curvature makes the deposits less stable. Alternatively, it can be pointed out that Ag atoms on small clusters have on the average lower coordination than on big clusters, so they become less stable. On the other hand, we

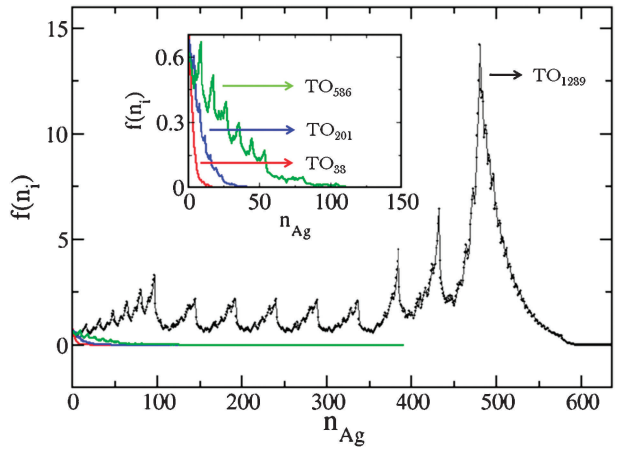

Fig. 7 Probability of observing n_{Ag} atoms deposited on Au(core) truncated octahedral nanoparticles of different sizes at zero excess of Ag chemical potential. The inset shows a zoom at small n_{Ag}.

have found that the existence of a negative curvature, as it is the case of a nanocavity, may act as a promoter for underpotential deposition.[29]

Conclusions

In the present work we presented a mechanical statistical formulation devised to analyze nanoparticle decoration by a foreign metal in terms of the interactions between the particles of the system.

Calculations were performed for a model system, and some interesting conclusions can be drawn:

- The most important contribution to the excess of free energy determining the stability of the decorated nanoparticle stems from the excess of internal energy. The other contributions (kinetic, rotational, and vibrational) are orders of magnitude smaller. Entropic effects are expected to become increasingly important for small nanoparticles.
- The type of decoration that can be achieved may depend strongly on nanoparticle size. While in the larger nanoparticles decoration of different facets may be achieved by control of the excess of chemical potential in the undersaturation region, in the case of small nanoparticles no decoration at all may be found under similar conditions.
- In the case of the electrochemical system, the previous point means a shift from underpotential to overpotential deposition on nanoparticles by changing nanoparticle size. This effect is expected to occur for small systems (NP of the order of 1000 atoms, which corresponds to an average diameter of approximately 3 nm).
- In the case of relatively large nanoparticles, metastable core-shell states may survive relatively large oversaturation conditions. Electrochemically speaking, overpotentials of the order of 150 mV.
- The present modeling may be extended to alloyed systems as well. In this case, the main problem will be to find the suitable configurations to calculate the canonical contributions to the Grand Canonical partition function.
- In many cases metallic nanoparticles of the size studied here (1–2 nm) are stabilized by a capping agent (*i.e.* thiols, amines, polymers) to avoid aggregation and sintering. In those cases where the interaction between the capping agent is relatively small as compared with the metal–metal bond (0.1 eV/atom or less) the presence of the capping agent would only add a (small) plus to the binding energy of the adsorbate atoms and the results of the calculations should be at least qualitatively valid. On the other hand, the present modeling may be generalized to introduce the effects of capping species by introducing Grand Canonical conditions for the latter. This work is in progress.

Appendix

In the present Appendix, we compare analytical entropy calculations with numerically exact results for a 4 × 6 patch of Au(100) surface at different Ag coverages. Periodic boundary conditions (PBC) were applied to this surface. The entropy of this system was calculated exactly though the equation:

$$S_{ex}(\Theta) = -k\sum_i P_i \ln P_i \qquad \text{(a1)}$$

with:

$$P_i = \frac{e^{-E_i/kT}}{\sum_i e^{-E_i/kT}} \qquad \text{(a2)}$$

where the sum runs over all the energy states compatible with the coverage degree Θ. In the present calculation this sum involved 16 777 216 configurations. This exact result was compared with the result of the calculation for $T \to 0$ K, denoted with $S_{T=0}$, where the probability was calculated on the basis of straightforwardly hand counting the number of the most compact equivalent structures at each coverage. We performed these entropy calculations using two types of interaction potentials: EAM potentials and pair potentials yielding the same interaction energy between nearest neighbors as the EAM ones.

Fig. 8a shows $S_{ex}(\Theta)$ at $T = 300$ K calculated using the EAM potentials and $S_{T=0}$. It is found that the $T = 0$ K calculation somehow underestimates the entropy values. However, they deliver the correct order of magnitude. The reason for this underestimation is mainly grounded on the many-body nature of the potential, where the second nearest neighbor can play an important role in delivering more structures with a similar energy.

This can be shown by considering the analogous problem using (Ising like) pair potentials. Fig. 8b shows configurational entropy calculations performed using pair potentials with a pair interaction of −0.25 eV at 300 K and 1000 K. It is found that the results for 300 K are indistinguishable from the analytical ones.

We now turn to perform a crude estimation of the configurational entropy of the different systems on the basis of considering the more compact structure for a given coverage degree.

Let us consider a square lattice with M sites with periodic boundary conditions, with a compact structure of N atoms adsorbed on it. If the structure made of N atoms is perfectly square, the entropy will be given by:

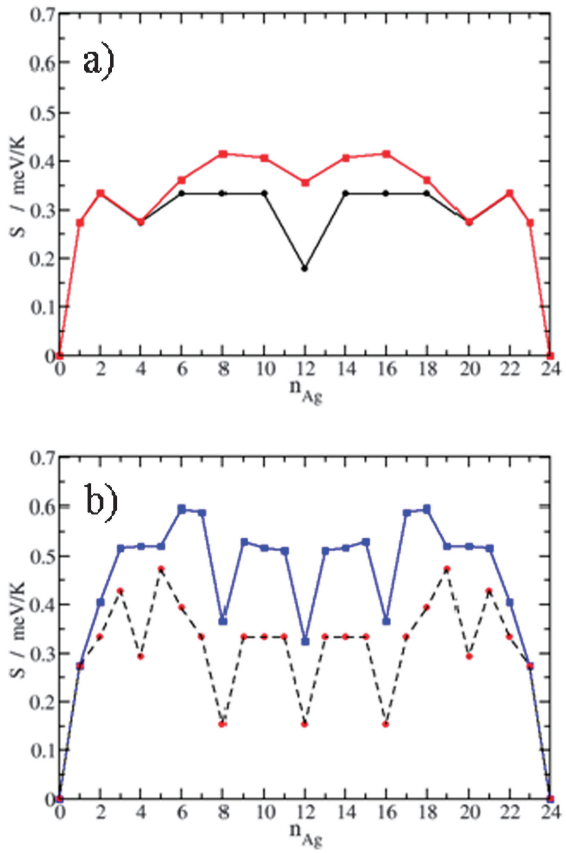

Fig. 8 Configurational entropy as a function of the number of Ag atoms deposited on a Au(4 × 6) substrate. (a) Using eqn (a1) with EAM potentials at 300 K (red squares); and hand counting the number of states (black circles). (b) Using eqn (a1) with "Ising like" pair potentials at 300 K (red dots), at 1000 K (blue squares) and hand counting the number of states (black dotted line).

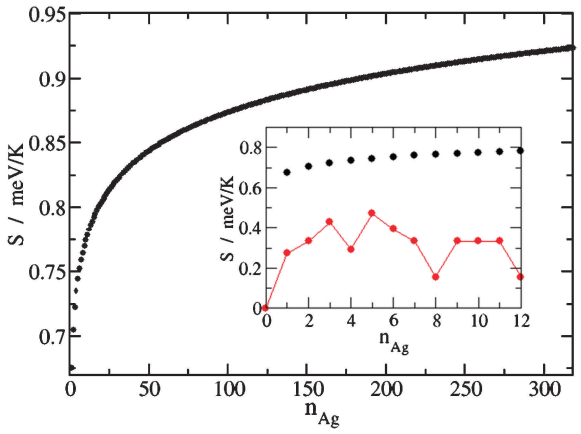

Fig. 9 Configurational entropy at a function of the number of substrate sites, calculated according to eqn (a4). The inset compares the results for the Fig. A1b (red line and dots) with the configurational entropy upper bound given in eqn (a4) (black dots).

$$S_{T=0} = k\ln M \qquad \text{(a3)}$$

since the square may be located on any of the M sites of the lattice with PBC. On the other hand, if the adsorbate consists of a square surrounded by some atoms, its entropy will be roughly given by:

$$S_{T=0} = k\ln[M(4N^{1/2})] \qquad \text{(a4)}$$

where $4N^{1/2}$ makes reference to the number of different sites available at the perimeter of the square of side $N^{1/2}$. Since the eqn (a4) is an upper bound of eqn (a3), we will use it to estimate the order of magnitude of the entropy for the different structures.

Fig. 9 shows the behavior of eqn (a4) for a system with a number of adsorption sites (636) similar to that of the largest NP considered in the body of the present work. In the inset, we give the results for the small system considered above in Fig. 8 as compared with the exact results at 300 K.

We can conclude that the largest configurational entropy contribution of the present core-shell system, delivers a contribution to the free energy of the system of the order of 0.3 eV at room temperature, being thus negligible as compared with the energetic contributions.

Acknowledgements

Authors wish to offer thanks for the financial support of the Consejo Nacional de Investigaciones Científicas y Técnicas (CONICET), Secyt UNC, Programs BID PICT 2006 PICT No 946 and PICT No 00340. O. A. Oviedo thanks CONICET for the fellowship.

References

1 A. S. Barnard, *J. Phys. Chem. B*, 2006, **110**, 24498.
2 A. S. Barnard, N. P. Young, A. I. Kirkland, M. A. van Huis and H. Xu, *ACS Nano*, 2009, **3**, 1431.
3 R. Ferrando, J. Jellinek and R. L. Johnston, *Chem. Rev.*, 2008, **108**, 845.
4 M. C. Daniel and D. Astruc, *Chem. Rev.*, 2004, **104**, 293.
5 *Recent Advances in Nanoscience*, ed. M. M. Mariscal and S. A. Dassie, Research Signpost, Trivandrum, Kerala, India, 2007.
6 J. Park, J. Joo, S. G. Kwon, Y. Jag and T. Hyeon, *Angew. Chem., Int. Ed.*, 2007, **46**, 4630.
7 T. Sugimoto, Elsevier, 2001.
8 T. L. Hill, *Thermodynamics of small systems, Part I and II*, Dover, 1994.
9 T. L. Hill and R. V. Chamberlin, *Proc. Natl. Acad. Sci. U. S. A.*, 1998, **95**, 12779.
10 Q. Jiang, X. H. Zhou and M. Zhao, *J. Chem. Phys.*, 2002, **117**, 10269.
11 C. X. Wang, Y. H. Yang, N. S. Xu and G. W. Yang, *J. Am. Chem. Soc.*, 2004, **126**, 11303.
12 E. Mendez-Villuendas, I. Saika-Voivod and R. K. Bowles, *J. Chem. Phys.*, 2007, **127**, 154703.
13 W. J. Plieth, *J. Phys. Chem.*, 1982, **86**, 3166.
14 R. Shuttleworth, *Proc. Phys. Soc., London, Sect. A*, 1950, **63**, 444.
15 A. I. Rusanov and A. Shchekin, *J. Chem. Phys.*, 2007, **127**, 191102.
16 E. Budevski, G. Staikov and W. J. Lorenz, *Electrochemical Phase Formation and Growth*, VCH, 1996.
17 O. A. Oviedo, M. M. Mariscal and E. P. M. Leiva, *Phys. Chem. Chem. Phys.*, 2008, **10**, 3561.
18 G. Staikov and W. J. Lorenz, in *Electrochemical Nanotechnology—In situ Local Probe Techniques at Electrochemical Interfases*, ed. W. Pliethy and W. J. Lorenz, Wiley-VCH, 1998.
19 T. L. Hill, *Introduction to Statistical Thermodynamics*, Addison-Wesley, 1962.
20 E. P. M. Leiva, *Electrochim. Acta*, 1996, **41**, 2185.
21 R. A. Johnson, *Phys. Rev. B: Condens. Matter*, 1989, **39**, 12554.
22 M. I. Rojas, C. G. Sanchez, M. G. Del Pópolo and E. P. M. Leiva, *Surf. Sci.*, 2000, **453**, 225.

23 O. A. Oviedo, M. I. Rojas and E. P. M. Leiva, *Electrochim. Acta*, 2006, **51**, 3526.
24 Y. H. Chui, G. Grochola, I. K. Snook and S. P. Russo, *Phys. Rev. B: Condens. Matter Mater. Phys.*, 2007, **75**, 033404.
25 F. Baletto and R. Ferrando, *Rev. Mod. Phys.*, 2005, **77**, 371 and references therein.
26 C. M. Wei, C. Cheng and C. M. Chang, *J. Phys. Chem. B*, 2006, **110**, 24642.
27 K. Koga, T. Ikeshoji and K. Sugawara, *Phys. Rev. Lett.*, 2004, **92**, 115507.
28 J. Zhang, Y. Tang, L. Weng and M. Ouyang, *Nanoletters*, 2009, **9**, 4061.
29 N. B. Luque, L. Reinaudi, P. Serra and E. P. M. Leiva, *Electrochim. Acta*, 2009, **54**, 3011.